Atmos. Chem. Phys., 12, 6405–6416, 2012
www.atmos-chem-phys.net/12/6405/2012/
doi:10.5194/acp-12-6405-2012

Atmospheric Chemistry and Physics

CO_2 flux estimation errors associated with moist atmospheric processes

N. C. Parazoo[1], A. S. Denning[2], S. R. Kawa[3], S. Pawson[3], and R. Lokupitiya[4]

[1]Jet Propulsion Laboratory, California Institute of Technology, Pasadena, CA, USA
[2]Department of Atmospheric Science, Colorado State University, Fort Collins, Colorado, USA
[3]NASA Goddard Space Flight Center, Greenbelt, Maryland, USA
[4]Department of Statistics and Computer Science, University of Sri Jayawardenepura, Gangodawila, Nugegoda, Sri Lanka

Correspondence to: N. C. Parazoo (nicholas.c.parazoo@jpl.nasa.gov)

Received: 3 April 2012 – Published in Atmos. Chem. Phys. Discuss.: 18 April 2012
Revised: 25 June 2012 – Accepted: 1 July 2012 – Published: 24 July 2012

Abstract. Vertical transport by moist sub-grid scale processes such as deep convection is a well-known source of uncertainty in CO_2 source/sink inversion. However, a dynamical link between vertical transport, satellite based retrievals of column mole fractions of CO_2, and source/sink inversion has not yet been established. By using the same offline transport model with meteorological fields from slightly different data assimilation systems, we examine sensitivity of frontal CO_2 transport and retrieved fluxes to different parameterizations of sub-grid vertical transport. We find that frontal transport feeds off background vertical CO_2 gradients, which are modulated by sub-grid vertical transport. The implication for source/sink estimation is two-fold. First, CO_2 variations contained in moist poleward moving air masses are systematically different from variations in dry equatorward moving air. Moist poleward transport is hidden from orbital sensors on satellites, causing a sampling bias, which leads directly to small but systematic flux retrieval errors in northern mid-latitudes. Second, differences in the representation of moist sub-grid vertical transport in GEOS-4 and GEOS-5 meteorological fields cause differences in vertical gradients of CO_2, which leads to systematic differences in moist poleward and dry equatorward CO_2 transport and therefore the fraction of CO_2 variations hidden in moist air from satellites. As a result, sampling biases are amplified and regional scale flux errors enhanced, most notably in Europe (0.43 ± 0.35 PgC yr^{-1}). These results, cast from the perspective of moist frontal transport processes, support previous arguments that the vertical gradient of CO_2 is a major source of uncertainty in source/sink inversion.

1 Introduction

Measurements of atmospheric CO_2 mixing ratio contain information about land and ocean carbon sinks, which act as natural buffers against rising fossil fuel emissions. Flux inversion methods combine information from winds, CO_2 measurements, and surface flux estimates to infer the size and distribution of these sinks (e.g., Gurney et al., 2002). Continuous records residing in the continental boundary layer close to terrestrial ecosystems allow quantitative flux estimation at finer spatial scales then previously possible (e.g., Law et al., 2003; Peylin et al., 2005; Zupanski et al., 2007; Lauvaux et al., 2009; Schuh et al., 2010), while spaced-based measurements of total column CO_2 help fill critical gaps in the in-situ network (Baker et al., 2010; Chevallier et al., 2010). Nevertheless, model transport error, specifically related to sub-grid scale vertical transport, remains a well-known but poorly characterized source of uncertainty in source/sink inversions of surface and column CO_2 data (Denning et al., 1999; Yi et al., 2004; Yang et al., 2007; Stephens et al., 2007; Houweling et al., 2010; Chevallier et al., 2010; Liu et al., 2011).

In the era of satellite measurements, an additional complication arises because the strongest horizontal gradients in CO_2 occur along frontal boundaries that are typically hidden from orbital sensors by clouds (Corbin and Denning, 2006), leading to systematic sampling errors of up to 1.5 ppm at seasonal scales (Corbin and Denning, 2008). Because a significant portion of the synoptic signal is correlated with moist processes and therefore likely to be unobserved by satellites (Parazoo et al., 2011), covariance of moist transport with surface CO_2 flux will cause errors in top-down flux estimates if not represented correctly in transport models.

Published by Copernicus Publications on behalf of the European Geosciences Union.

In this study we quantify differences in forward calculations of moist frontal CO_2 transport and examine the impact on source/sink inversion. Forward simulations are run using a common tracer transport model and identical surface fluxes, but with transport driven by meteorological fields from four versions of the National Atmospheric Space Administrations' Goddard Earth Observing System Data Assimilation System (GEOS-DAS). The four resulting simulations are analyzed in terms of eddy and mean meridional mass fluxes of CO_2, which are calculated using eddy decomposition (Parazoo et al., 2011). This approach characterizes moist frontal CO_2 transport into a single term, which can be used as a diagnostic for inter-model comparison. Uncertainty in frontal transport is quantified as the spread in forward calculations of eddy transport.

Unique aspects of forward simulations include the use of an identical tracer model, identical surface fluxes, and analyzed meteorological fields derived from a common general circulation model (GCM). Conversely, intercomparison studies that use a wider set of models are often unable to account for sensitivity to a wide range of factors, including differences in dynamical core, meteorological analysis fields, coordinate systems, and surface fluxes. While no forward simulation of CO_2 is flawless, here we are at least able to account for sensitivity of moist frontal CO_2 transport to an isolated set of factors, specifically horizontal grid spacing and subgrid scale vertical transport due to moist convection and vertical diffusion.

We also examine the impact of model differences in moist frontal transport on the inversion of total column CO_2 retrievals from satellite remote sensing instruments using Observation System Simulation Experiments, or OSSE's. Several OSSE's are presented in order of increasing complication, first to establish baseline flux retrieval errors due to optimization and data screening, then to examine the degree to which signal detection is possible, and finally to evaluate sensitivity of signal detection to model transport. Each OSSE has two primary steps: (1) the nature run, in which synthetic retrievals of column CO_2 are created by sampling forward simulations according to the Greenhouse gases Observing SATellite (GOSAT) (e.g., Kuze et al., 2009), and (2) the inversion run, in which CO_2 fluxes are recovered from synthetic retrievals using ensemble optimization.

OSSE's are similar in design to Chevallier et al. (2010) in that one set of experiments use a common set of meteorological fields for transport in Steps 1 and 2 and another set examines transport bias by using different meteorological fields in Steps 1 and 2. Several key differences are as follows: (1) the current study uses the same transport model in all experiments, eliminating sensitivity to differences in numerical integration; (2) meteorological fields are derived from very similar data assimilation systems but using uniquely different representations of sub-grid vertical transport; (3) use of ensemble data assimilation framework and estimation of systematic biases to component fluxes (technique described in Lokupitiya et al., 2008 and references therein); (4) a subset of end-to-end OSSE calculations are performed to quantify baseline errors in the inversion system, in particular due to temporal sampling errors, before errors related to transport uncertainty are analyzed; and (5) an attempt to understand whether differences in retrieved fluxes can be attributed to specific dynamical differences in meteorological fields. This last point is key: rather than point out when and where flux retrieval errors occur, we attempt to explain flux errors from a dynamical viewpoint. We note that despite increasing complexity, OSSE's are highly simplified; for example, the effect of changes in aerosol optical depth and land surface type on XCO_2 retrievals is not considered. Given the similarity of experiments yet uniqueness of methods, Chevallier et al. (2010) provide an excellent benchmark for comparison.

2 Methods

2.1 Forward Simulations

Global CO_2 transport is analyzed in the Parameterized Chemistry and Transport Model (PCTM, see Kawa et al., 2004). Surface fluxes, described in Parazoo et al. (2008), are the same for each simulation, and include air-sea exchange, constant in time fossil fuel emissions, and a steady state terrestrial biosphere. These fluxes are also used as "priors" in Step 2 of the source/sink inversion experiments (see Sect. 2.3). PCTM is run from 1 January 2000 through 31 December 2004 to spin up atmospheric gradients of CO_2 and create a common initial condition, and from 1 January 2005 through 31 December 2005 using the four reanalysis products (described below) to comprise the analysis period.

Transport in the PCTM is computed off-line using archived meteorological analyses from different versions of the GEOS DAS. Two distinctly different GEOS analyses, Versions 4 and 5, are used in this study. These meteorological analyses differ in (1) physical parameterizations in the GCM; (2) native resolution; (3) the algorithm used for the meteorological analysis; and (4) the manner in which the analyses are assimilated with the GCM. The physical parameterizations in the GEOS-4 GCM are substantially different from GEOS-5 (see below). GEOS-4 has a native resolution of $1.25^\circ \times 1^\circ$ (longitude $\times$ latitude) and 55 layers while GEOS-5 has a native resolution of $0.67^\circ \times 0.5^\circ$ and 72 layers. Most of the additional layers in GEOS-5 are in the troposphere. This study uses meteorological datasets saved at the native resolution of each of these forecast models. We also use two additional datasets that are saved at a reduced resolution, giving a total of four meteorological datasets based on the same dynamical core to transport CO_2. The different analysis techniques are likely to impact simulations, but isolating this factor is difficult in an offline framework. We therefore focus on the impact of horizontal grid spacing and sub-grid transport on forward simulations of CO_2 transport, keeping in mind

Table 1. Description of meteorological datasets used in offline tracer transport simulations. Column 1 (Data) is the code name for the meteorological dataset, 2 (Version) is the version of the analysis product, 3 (Native Resolution) is the resolution at which the analysis system (forecast + assimilation) is run ($a \times b \times c$ = latitude spacing × longitude spacing × number of vertical levels), 4 (Transport Resolution) is the grid spacing at which the analysis is saved, 5 (Full or Reduced) refers to whether the analysis is saved at the native resolution of the parent GCM or interpolated to a coarser resolution, 6 (Deep Convection) is the deep convection scheme of the parent GCM, and 7 (Turbulence) is the PBL turbulence scheme of the parent GCM. Naming convention for analysis product in the first column is as follows: character 1–2 is the product version number (G4 = GEOS-4 and G5 = GEOS-5), character 3 is the grid at which the analysis is saved (F = full resolution and R = reduced resolution), and character 4–5 is the latitude grid spacing at which the analysis is saved for offline transport (05 = 0.5°, 10 = 1.0°, 20 = 2.0°).

Run	Version	Native Resolution	Transport Resolution	Full or Reduced	Deep Convection	Turbulence
G5F05	5.1.0	0.5° × 0.67° × 72	0.5° × 0.67° × 42	Full	Moorthi and Suarez (1992)	Louis et al. (1982) Lock et al. (2000)
G5R10	5.2.0	0.5° × 0.67° × 72	1.25° × 1.0° × 42	Reduced (regridded from G5F05)	Moorthi and Suarez (1992)	Louis et al. (1982) Lock et al. (2000)
G4F10	4.5.3	1.25° × 1.0° × 55	1.25° × 1.0° × 25	Full	Zhang and McFarlane (1995)	Holtslag and Boville (1993)
G4R20	4.5.3	1.25° × 1.0° × 55	2.5° × 2.0° × 25	Reduced (regridded from G4F10)	Zhang and McFarlane (1995)	Holtslag and Boville (1993)

sensitivity to other factors. The key differences between these models are summarized in Table 1 and specified in more detail below.

The GEOS-4 analysis (Bloom et al., 2005) procedure uses the Physical-space Statistical Analysis Scheme of Cohn et al. (1998), which produces an optimal combination of six-hour model forecasts and observations at the observation locations. These are interpolated to the model grid and the model background fields (surface pressure, winds, temperature and moisture) are replaced with the analyses every six hours. Six-hour time-averaged GEOS-4 fields are used in the present study (Pawson et al., 2007). Physical parameterizations in GEOS-4 are drawn from the National Center for Atmospheric Research Community Climate Model, Version 3 (CCM3) package (Kiehl et al., 1998), which include deep convection (Zhang and McFarlane, 1995), shallow convection (Hack, 1994), and Planetary Boundary Layer (PBL) turbulence (Holtslag and Boville, 1993).

GEOS-5 analyses (Rienecker et al., 2008) use a three-dimensional variational approach in gridpoint space (Gridpoint Statistical Analysis, GSI, Wu et al., 2002) that directly assimilates satellite radiances alongside the conventional meteorological data. These analyses are input smoothly into the GEOS-5 GCM, using the incremental analysis update (IAU) approach of Bloom et al. (1996): this involves adding additional forcing terms to the momentum, thermodynamic and moisture tendencies, which are the local (gridpoint) forces needed to drive the background forecasts to the analyses over the six-hour window of the assimilation. This method of merging the analyses to the model leads to smoothly varying fields in the assimilation, which means that the transport in GEOS-5 is much smoother than in GEOS-4. The GEOS-5 GCM maintains the finite-volume dynamics used in GEOS-4 (Lin, 2004) and is integrated with physics packages under the Earth System Modeling framework (e.g., Collins et al., 2005), including the Relaxed Arakawa-Schubert (RAS) scheme for convection (Moorthi and Suarez, 1992) and separate PBL turbulent mixing schemes for stable (Louis et al., 1982) and unstable (Lock et al., 2000) conditions.

2.1.1 G4F10

The first analysis used in this study is the GEOS-4 DAS, as implemented by Kawa et al. (2004) in the original PCTM study of CO_2 transport. Meteorological fields from GEOS-4 DAS are saved every 6 h at the native resolution of 1.25° by 1°, with 55 hybrid vertical levels up to 0.01 hPa. Only 25 levels are used for transport in PCTM, although all levels in the troposphere are retained. This re-analysis driver data will be referred to as G4F10. 1.25° by 1° transport in PCTM is run with a 7.5 min time step.

2.1.2 G4R20

G4F10 is regridded horizontally to 2.5° by 2° to study transport at coarser grid spacing. Vertical mixing by moist convection and turbulent diffusion is identical to G4F10. Vertical and horizontal advection is conserved, leading to smoothed spatial gradients. All 25 vertical levels are retained, and transport fields are saved at 6-hourly resolution.

Time-stepping through PCTM is doubled to 15 min. This regridded version of G4F10 is referred to as G4R20.

2.1.3 G5F05

The third product is based on version 5 of GEOS-DAS (GEOS-5 DAS, Rienecker et al., 2008). Native grid spacing and sub-grid vertical mixing are key differences from GEOS-4. This first GEOS-5 product is from Version 5.1.0, which was run for the period 1 October 2003–2 October 2008 in support of NASA's science missions. The native grid of GEOS-5 DAS (the grid at which the analysis is performed) is 0.67° by 0.5° in the horizontal with 72 layers to 0.01 hPa, 31 of which are in the troposphere. The 72 vertical layers are reduced to 42 levels while retaining the 31 tropospheric levels. Instantaneous transport fields are saved at 6-hourly resolution. Reduced grid spacing requires a time step of 3.75 min. This driver data is referred to as G5F05.

2.1.4 G5R10

The fourth product is similar to G5F05 except with a newer version (5.2.0) of GEOS-5 DAS used for the Modern-Era Retrospective analysis for Research Applications (MERRA) (Rienecker et al., 2011). The system contains several improvements from the GEOS-5.1.0 system (Rienecker et al., 2008), including tuning of the sub-grid physical packages and aspects of the GSI analysis system. Transport fields are re-analyzed (saved during a corrector segment of the Incremental Analysis Update rather than the analysis segment) and saved every 3 h at a reduced horizontal resolution of 1.25° by 1°. This facilitates comparison with the G4F10 dataset, although it should be noted that analyses with GEOS-5 performed at the 1.25° by 1° resolution differ in important ways from the data that are interpolated to that resolution. This re-analyzed driver data will be referred to as G5R10.

2.2 Calculations of frontal CO_2 transport

Eddy decomposition of CO_2 transport is described in more detail by Parazoo et al. (2011); here we provide a brief description. Frontal CO_2 transport is diagnosed by parsing total column integrated meridional CO_2 transport as described by PCTM into eddy and mean components of the large-scale atmospheric circulation. The eddy component arises from correlated variations of mass flux and CO_2 mixing ratio. Frontal passage events are transient and migrating, tend to deviate strongly from the mean overturning circulation (e.g., Hadley Cell), and are therefore associated with strong variations of mass flux. When CO_2 gradients align with frontal air parcel trajectories along the meridional plane, the eddy component amplifies. These conditions are often satisfied in northern mid-latitudes (Keppel-Aleks et al., 2011). The vertical coordinate that describes frontal transport is also critical because variations of atmospheric fields are sensitive to trajectory. In order to capture moist ascent of air parcels along stormtracks (e.g., Pauluis et al., 2008), the analysis therefore relies on the calculation of eddy and mean transport on moist isentropic surfaces, which conserve energy as rising air condenses and releases latent heat.

2.3 Synthetic inversion experiments

The inversion system uses an ensemble-based approach to data assimilation referred to as the Maximum Likelihood Ensemble Filter (MLEF; Zupanski et al., 2007; Lokupitiya et al., 2008). The strategy for flux estimation is based on the idea that high frequency variations in respiration and photosynthesis are driven by relatively well-understood and easily modeled processes that are determined to first order by variations in solar radiation (Zupanski et al., 2007), while slowly varying processes (e.g., nitrogen deposition) are typically not modeled as well and lead to persistent biases in CO_2 exchange. We therefore prescribe hourly, synoptic, and seasonal variations in terrestrial CO_2 flux from models, and allow the inversion to solve for persistent biases at grid scale due to nitrogen deposition in northern mid-latitudes and CO_2 fertilization in the tropics.

Biases are assumed to be constant over the length of the data assimilation window. Lokupitiya et al. (2008) solved for 8-week biases by assimilating synthetic surface data over the same period. This assimilation window was found to reasonably recover fluxes given a sparse measurement network (Peters et al., 2005). Although this window is short relative to the length of time needed to effectively capture signals from source regions (Bruhwiler et al., 2005), this extra information is mostly diluted by atmospheric mixing and comes at a greater computational cost. Satellite observing systems such as GOSAT greatly improve spatial coverage, and thus longer windows may not be required. Here, we consider a 2-week window. Given the short assimilation window and grid scale inversion, strong covariance smoothing is applied at the first cycle of MLEF, using e-folding length of 800 km over land points and 1600 km over ocean points. Further details regarding the assimilation scheme are discussed by Lokupitiya et al. (2008).

GOSAT uses a sun-synchronous orbit with early afternoon sun-lit equator crossing time ($\sim$01:30 p.m. LT) and orbital inclination near 98°. Synthetic GOSAT retrievals are generated in forward simulations of the nature run (Step 1) using pressure-weighted column averaging of vertical CO_2 profiles. Since GOSAT measures CO_2 absorption using reflected solar radiation, PCTM is sampled only during daytime of the descending mode of orbit. Subsequent orbits are separated by $\sim 25°$ in longitude and ~ 99 min apart. GOSAT points near-nadir as well as at the sun glint spot, which greatly increases the signal over the ocean. We assume a 5-point cross-scan track, which was used on GOSAT between 4 April 2009 and 31 July 2010, with footprints separated by ~ 158 km cross-track and ~ 152 km along track (Crisp et

Table 2. Summary of OSSE's used in source/sink inversions. Red shading refers to "perfect transport" experiments, green "signal detection", and blue "biased transport". The "true" flux refers to the set of surface CO_2 fluxes prescribed in Step 1. The "prior" flux refers to surface fluxes used as a first guess in Step 2. Prior fluxes are described in Parazoo et al. (2008), and include a steady state terrestrial biosphere. This means that the true flux in Experiments 1, 2 and 5 is the same as the prior flux used in Step 2, while the true flux in Experiments 3, 4 and 6 also includes a globally distributed 3 PgC sink (see Fig. 7a).

Experiment	Observation Transport (Step 1)	Inversion Transport (Step 2)	True Flux	Cloud Screening
1	GEOS-4	GEOS-4	Prior	No
2	GEOS-4	GEOS-4	Prior	Yes
3	GEOS-4	GEOS-4	Prior + Constant 3 PgC Sink	Yes
4	GEOS-4	GEOS-4	Prior + Seasonal 3 PgC Sink	Yes
5	GEOS-5	GEOS-4	Prior	Yes
6	GEOS-5	GEOS-4	Prior + Seasonal 3 PgC Sink	Yes

al., 2012). Soundings are sampled at the native resolution of the meteorological analysis in the nature run (see below) at 01:30 p.m. LT, and are assumed to represent the grid scale average. No temporal averaging of synthetic retrievals is applied. A maximum of 281 points are sampled by GOSAT in one hour, corresponding to 94 416 points over the 2-week assimilation period. All possible glint retrievals are retained, including those beyond $\pm 20^\circ$ of latitude from solar declination. In practice, however, glint mode is only used by GOSAT at latitudes within 20° of latitude from solar declination. We therefore run an additional OSSE in the signal detection experiment (Experiment 3, described below) to test for the impact of high latitude glint data on flux recovery. We prescribe a uniform uncertainty of 3 ppm to GOSAT retrievals; this is chosen as an upper bound from values computed by Chevallier et al. (2009) due to measurement noise, smoothing error, interference error component, and overall random contribution of aerosols to retrieval noise.

Clear conditions are defined as grid cells with cloud optical depth less than 0.3. Aerosol effects are not considered in this study. Cloud optical depth is prescribed from MERRA and defined as the grid scale value (total in-cloud optical depth from ice and liquid water times the three dimensional total cloud fraction in a grid box). MERRA estimates of clear-sky ratio compare favorably with CALIOP estimates from Eguchi and Yokota (2008) in northern middle and boreal latitudes and in tropical regions. MERRA tends to overestimate the percentage of clear sky days in southern Africa, Austrialia, the mid-continental portion of southern S. America near 30° S, over the Southern Ocean, and the Arctic. Cloud screening leads to greater than 90 % loss of data in most regions, especially in persistent cloudy areas in tropical and boreal latitudes.

A total of six OSSE's are reported in this study (see Table 2). Step 2 (inversion run) is identical for each OSSE, where MLEF is used for optimization, PCTM for offline transport, and G4R20 for meteorological forcing. Biases are therefore recovered at $2.5^\circ \times 2^\circ$ resolution. Step 1 differs in the prescription of the true flux and meteorological forcing. OSSE's 1 and 2 are "perfect transport" experiments, where G4R20 is used in Step 1. These experiments are simplified further in that the true flux consists of a steady state terrestrial biosphere, and are therefore designed to establish baseline flux recovery errors related to ensemble optimization, random measurement error, measurement density reduction due to cloud screening, and temporal sampling biases. OSSE's 3 and 4 are "signal detection" experiments, which also use G4R20 in Step 1 but where the true flux includes the steady state terrestrial biosphere plus a slowly varying and globally distributed 3 GtC sink. This sink represents the persistent bias in the steady state terrestrial biosphere as described above and in Zupanski et al. (2007). These experiments are designed to test whether slowly varying sinks due to poorly modeled processes such as nitrogen deposition and regrowing forests in northern middle latitudes and CO_2 fertilization in the tropics are recovered from synthetic satellite retrievals. Finally, OSSE's 5 and 6 are "biased transport" experiments, where G5R05 is used in Step 1, and are therefore designed to quantify transport-driven flux errors. OSSE 5 uses the true flux as described in OSSE's 1 and 2; OSSE 6 uses the true flux as described in OSSE 4.

3 Results

3.1 Transport differences

Column integrated meridional CO_2 transport is shown in Fig. 1. Total column transport is approximately conserved between meteorological analyses. In the annual average, there is net northward transport north of 50° N and net southward transport south of 50° N (Fig. 1a); this pattern is dominated by winter transport (Fig. 1b). The direction of eddy and

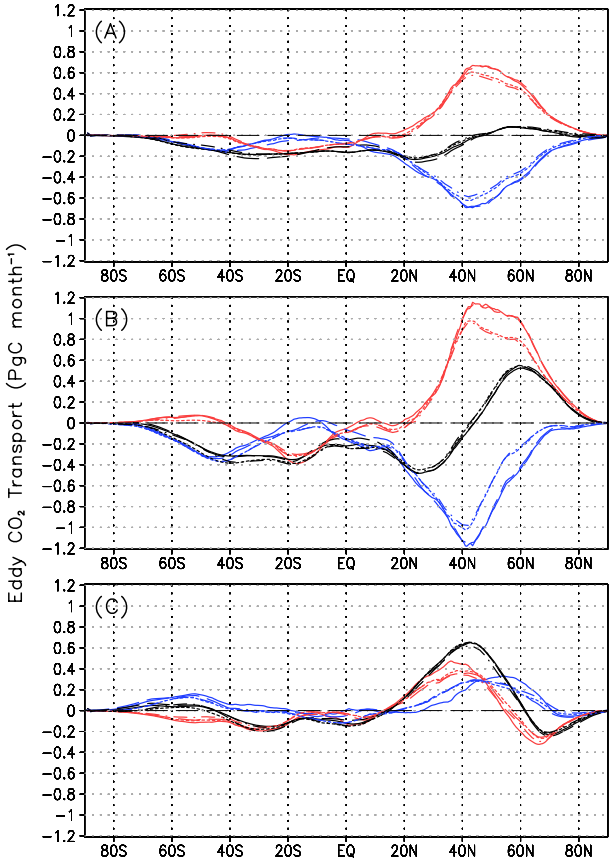

Fig. 1. Zonal-mean column integrated meridional CO_2 transport averaged over **(A)** 1 yr, **(B)** December-January-February and **(C)** June-July-August. Total meridional transport is shown in black, "mean" transport in blue, and "eddy" transport in red. Line styles correspond to transport by the four meteorological analyses, where G5F05 is cyan and solid, G5R10 as blue and dashed, G4F10 is green and dotted, and G4R20 is red and dash-dotted.

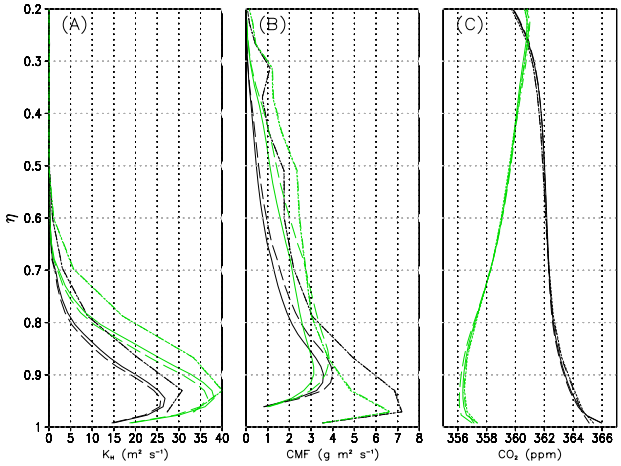

Fig. 2. Vertical profiles of **(A)** turbulent diffusion, **(B)** cumulus mass flux and **(C)** CO_2 mixing ratio, zonally averaged, binned into mid-latitudes (30–70° N) and plotted as a function of the hybrid coordinate eta (η) for each of the four meteorological analyses (line styles correspond to Fig. 1). Annual averages are plotted in black, summer averages in green. Mass fluxes from GEOS-4 are identical and therefore lie directly over one another. Note that vertical diffusion is zero in GEOS-4 at the lowest model level and cumulus mass flux is zero in GEOS-5 at the two lowest model levels.

mean CO_2 transport is independent of analyses. Eddy transport is on average poleward in both hemispheres and opposed by southward mean transport in northern latitudes. The direction of eddy and mean transport switches sign in summer north of 50° N (Fig. 1c), consistent with strong CO_2 uptake. The magnitude of transport by eddy and mean circulations is, however, quite sensitive to the analyses. For example, eddy transport in northern mid-latitudes (40–60° N) is generally stronger and more poleward in GEOS-5, exceeding transport in GEOS-4 by 0.1 PgC month^{-1} in the annual mean and close to 0.2 PgC month^{-1} during winter and summer.

GEOS-4 models differ only in horizontal grid spacing; transport differences between G4R20 and G4F10, although small, are therefore explained by regridding of G4F10 to the coarser grid of G4R20. Different transport in GEOS-5 models is also largely explained by differences in grid spacing, although data assimilation procedures and model physics updates between 5.1.0 and 5.2.0 (e.g., high latitude diurnal cycle) may also contribute. Transport differences between G4F10 and G5R10 are more complicated, and likely due to a combination of factors, including: (1) the representation of sub-grid scale processes, (2) horizontal/vertical grid spacing, (3) the new data assimilation system and (4) number and type of observational data assimilated.

Sub-grid scale processes are probably easiest to examine because mass flux coefficients for cumulus convection and turbulent diffusion are saved in the reanalysis. Vertical mass fluxes are plotted as a function of the terrain following coordinate η and averaged in northern mid-latitudes (30–70° N) in Fig. 2. Turbulent mixing (Fig. 2a) and cumulus convection (Fig. 2b) in GEOS-5 are consistently weaker than GEOS-4 throughout the column in northern mid-latitudes. Cumulus convection also starts higher in the PBL in GEOS-5 (Fig. 2b), reducing vertical transport from the surface. Weak vertical mixing in mid-latitudes in GEOS-5 is consistent with Ott et al. (2009), who found that single column model application of RAS-based moist convection significantly underestimates convective mass flux relative to cloud resolving models for several case studies of mid-latitude convective storms, resulting in weaker vertical transport of trace gases. The findings of Ott et al. (2009) were subsequently used to tune several key parameters in the convective parameterization of the GEOS-5 GCM (S. Pawson, personal communication, 2011). The effect of the tuning is apparent in the newer version of GEOS-5 (i.e., G5R10), where the vertical convective mass flux is larger than G5F05 in mid-latitudes while preserving the vertical distribution. Weaker vertical mixing

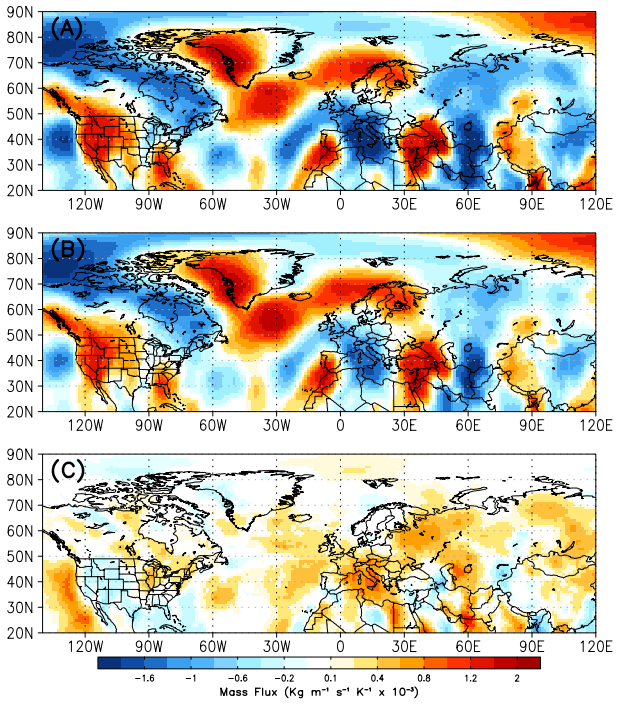

Fig. 3. Spatial structure of column integrated meridional mass flux averaged over the period June-July-August for **(A)** G4R20 and **(B)** G5F05. **(C)** Difference in meridional mass flux, or **(B)** minus **(A)**.

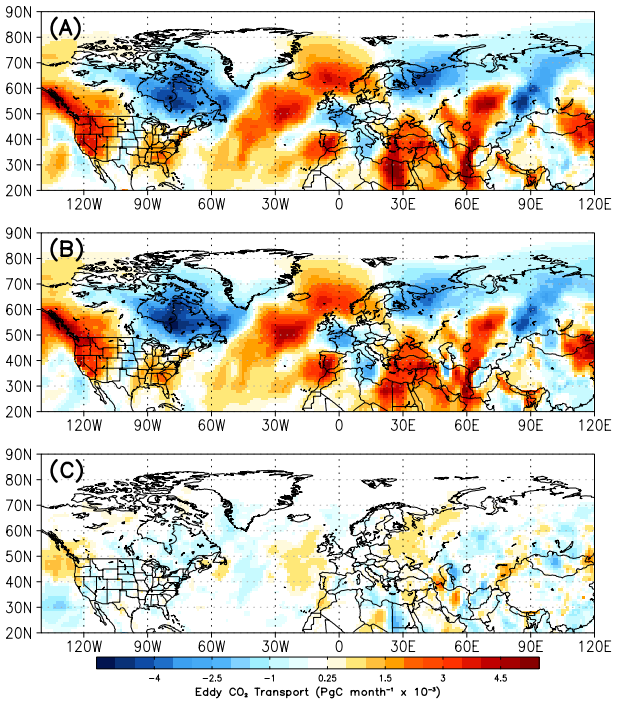

Fig. 4. Spatial structure of column integrated meridional eddy CO_2 transport averaged over the period June-July-August for **(A)** G4R20 and **(B)** G5F05. **(C)** Difference in eddy transport, or **(B)** minus **(A)**.

in GEOS-5 traps CO_2 near the surface (Fig. 2c), causing a stronger negative (positive) vertical CO_2 gradient in the lower troposphere ($\eta = 1$–0.9) in the annual (summer) average. Since cold fronts and moist conveyor belts embedded in synoptic storms move CO_2 upward and poleward (Parazoo et al., 2011), it follows that stronger vertical gradients in GEOS-5 enhance poleward eddy CO_2 transport.

Differences in meridional wind associated with the combined (and non-linear) effects of sub-grid vertical transport, grid spacing, and data assimilation also cause differences in eddy CO_2 transport (Fig. 3). Meridional mass fluxes in GEOS-4 and GEOS-5 have similar spatial patterns during boreal summer in northern mid-latitudes, but have regional differences in magnitude, especially in in regions of equatorward transport (blue shading). With the exception of enhanced poleward transport in eastern Europe (25–50° E), equatorward and poleward mass fluxes are typically weaker in GEOS-5. Nevertheless, eddy CO_2 transport is generally stronger in GEOS-5 throughout mid-latitudes (Fig. 4), suggesting that enhanced vertical CO_2 gradients associated with weaker sub-grid vertical mixing are the primary driver of enhanced eddy CO_2 transport in GEOS-5.

3.2 Source/sink inversion

The effect of differences in eddy transport on flux retrieval is tested in the following series of inversion experiments, starting with simplified "perfect transport" experiments. First, when all retrievals are retained (Experiment 1), we find that total annual flux errors, representing the difference between the recovered and true flux, are negligible ($< 0.1\,\mathrm{PgC\,yr^{-1}}$, Fig. 5a) and initial uncertainty is reduced by 50 % (Fig. 5b), indicating MLEF inversion is robust to numerical errors. Seasonal errors are also small and mostly random (Fig. 6a). These baseline errors are not sensitive to the initial distribution of ensembles or ensemble size (50–200 ensembles), and do not increase when synthetic retrievals are randomly screened. For example, removal of 67 % of data using a random filter produces spatial patterns similar to Fig. 6a.

Screening specifically for retrievals with cloud optical depth greater than 0.3 (Experiment 2) also eliminates more than 67 % of observations in many regions; however, such systematic screening leads to flux errors of up to $0.25\,\mathrm{PgC\,yr^{-1}}$ in the tropics and $0.19\,\mathrm{PgC\,yr^{-1}}$ in Europe (Fig. 5, medium blue), which in northern mid-latitudes are most prominent during boreal summer (Fig. 6). Flux errors in N. America also increase, but carry a dipole pattern and tend to cancel in the annual mean. We note that, while flux errors increase in Experiment 2, they are not statistically significant from errors in Experiment 1; for example,

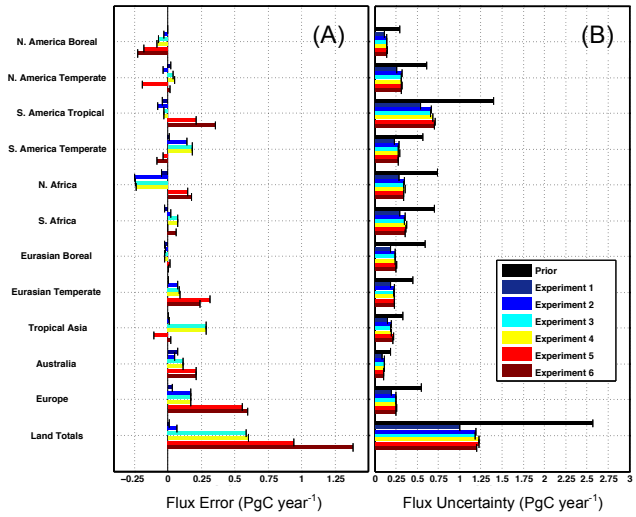

Fig. 5. Bar plots of total annual terrestrial flux error **(A)** and uncertainty **(B)** for Experiments 1–6, aggregated up to regional and global scale.

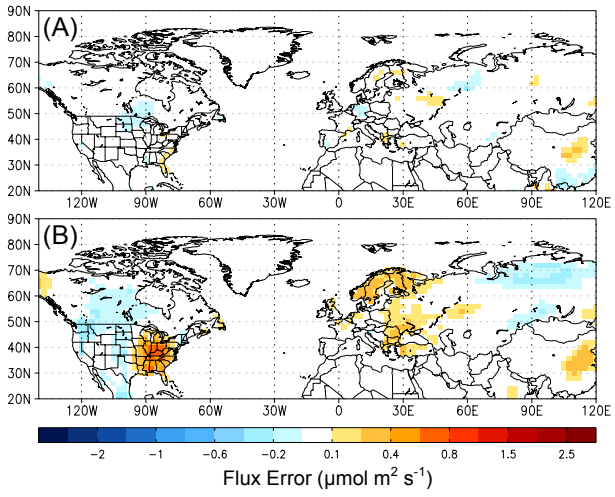

Fig. 6. Flux errors during boreal summer (June-July-August) in **(A)** Experiment 1 and **(B)** Experiment 2.

the difference between flux errors in Europe in Experiment 1 and 2 ($0.14\,\mathrm{PgC\,yr^{-1}}$) is well within the uncertainty in the difference ($0.32\,\mathrm{PgC\,yr^{-1}}$). Nevertheless, these results suggest that the size and spatial distribution of flux errors are more sensitive to the type, in contrast to quantity, of data removed.

Summertime flux errors in Europe and N. America (Fig. 6b) tend to be distributed in a way that aligns with patterns of poleward eddy CO_2 transport by G4R20 (Fig. 4a). For example, high CO_2 air is transported into the east half of N. America during summer through two mechanisms: upward and poleward moving moist conveyors in the south (red shading in the Southeast), which advect high CO_2 subtropical air residing in the lower troposphere, and downward and equatorward moving dry air intrusions from the north, which advect high CO_2 arctic air from the upper troposphere. Plots of column integrated meridional mass flux illustrate these air streams (Fig. 3a). While equatorward-moving air masses are typically dry and well sampled by satellites, poleward-moving air is moist and cloudy, causing an estimated 30 % of the underlying CO_2 air mass to be hidden in clouds from satellites (Parazoo et al., 2011), leading directly to a temporal sampling bias in the absence of surface observations. Although both air masses are high in CO_2, equatorward transport from the north is stronger. The air sampled by satellites is therefore enriched in CO_2 relative to average conditions, and the inversion compensates by creating a CO_2 "source" over N. America. A similar process of strong poleward transport of high CO_2 air in moist conveyors is responsible for the summer "source" in eastern Europe.

Despite these sampling biases, 80 % of the global 3.0 PgC sink represented by slowly varying processes in middle and tropical latitudes is recovered (Experiment 3, Fig. 5, cyan). Perturbing the sinks with spatial noise and seasonality does not degrade recovery (Experiment 4, Fig. 5, yellow), nor does removing glint retrievals exceeding $\pm 20°$ latitude of solar declination (with the exception of slightly enhanced source in northern Europe and reduced source in temperate S. America, not shown). The inversion also recovers the spatial distribution of sinks in N. America and tropical regions (Fig. 7). While the effect of the temporal sampling bias is clear in Europe, and reduces sink recovery in N. America, Experiments 3 and 4 illustrate that the bias recovery approach can separate slowly varying signals contained in column integrated CO_2 from high frequency signals, and then attribute these signals to the correct processes.

In "biased" transport OSSE's (Experiments 5 and 6), most regions experience an increase in total annual flux bias relative to baseline errors established in the equivalent "perfect" transport experiments (Experiments 2 and 4, respectively; see Fig. 5). For example in Experiment 5, Europe ($0.57 \pm 0.25\,\mathrm{PgC\,yr^{-1}}$), Eurasian Temperate ($0.32 \pm 0.23\,\mathrm{PgC\,yr^{-1}}$), and S. America Tropical ($0.21 \pm 0.71\,\mathrm{PgC\,yr^{-1}}$) contribute to an enhanced global source ($0.94 \pm 1.23\,\mathrm{PgC\,yr^{-1}}$), while N. America temperate and boreal regions contribute to an enhanced sink ($0.42 \pm 0.45\,\mathrm{PgC\,yr^{-1}}$). Eastern N. America reverses from a weak source in Experiment 2 (Fig. 6b) to a strong sink in Experiment 5 (Fig. 8). The global land source increases to $1.4\,\mathrm{PgC\,yr^{-1}}$ in Experiment 6 when slowly varying sinks are added (Fig. 5). The magnitude of flux errors in Experiment 6 is similar to Experiment 5 and consistent with Chevallier et al. (2010).

The difference between flux errors in perfect transport (Experiment 2 and 4) and biased transport (Experiment 5 and 6) experiments primarily reflect differences in transport.

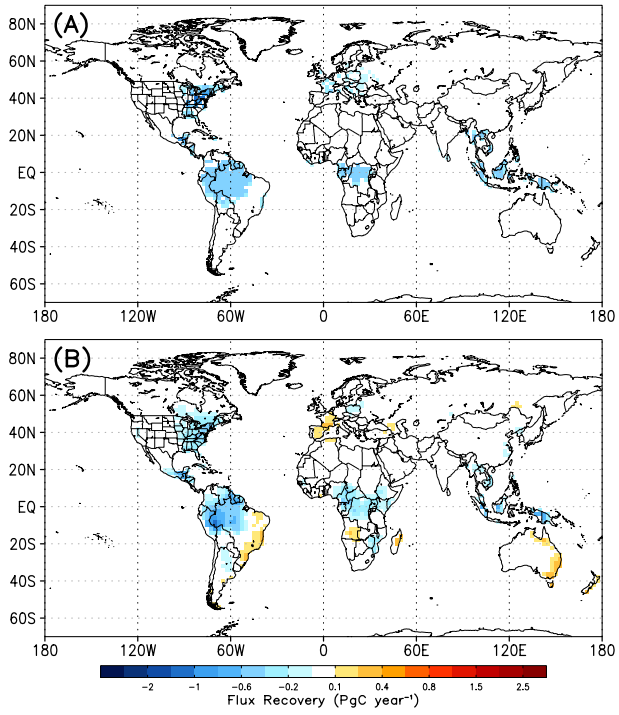

Fig. 7. (A) True and **(B)** recovered fluxes for Experiment 3, summed over one year.

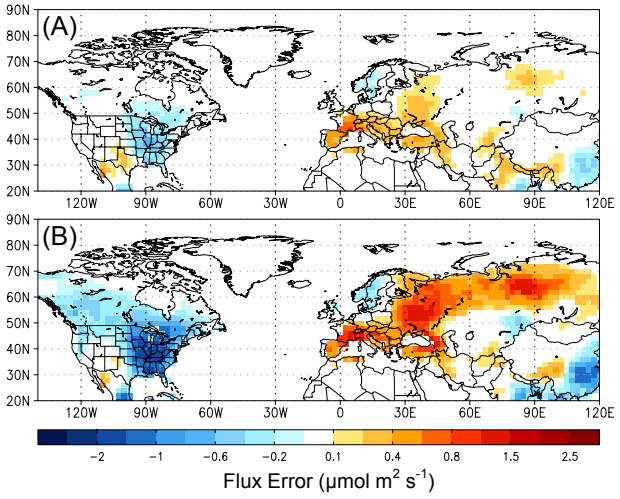

Fig. 8. Flux errors in Experiment 5, averaged over **(A)** 1 yr and **(B)** June-July-August.

Differences in the calculation of the dry air mole fraction of CO_2 due to differences in humidity fields between GEOS-4 and GEOS-5 are small in northern mid-latitudes (< 0.1 ppm at grid scale in the annual mean) and unlikely to contribute significantly to flux errors in N. America and Eurasia. With Experiment 6 as the reference and focusing on northern temperate and boreal regions, we therefore estimate that transport errors create a European source of 0.43 ± 0.35 PgC yr^{-1}, Eurasian Temperate source of 0.15 ± 0.32 PgC yr^{-1}, N. American Temperate sink of 0.04 ± 0.45 PgC yr^{-1}, and N. American Boreal sink of 0.15 ± 0.20 PgC yr^{-1}. The amplified European source is most significant relative to uncertainty between inversions.

Although high uncertainty between inversion experiments reduces the significance of source/sink amplification, these experiments reveal important sensitivities of flux estimates to transport patterns. In particular, systematic differences in eddy transport amplify temporal sampling bias in Europe and reverse the sign of bias in N. America. During N. America summer, G5F05 reduces poleward mass flux in the south (relative to G4R20) and equatorward mass flux in the north (Fig. 3c). While both processes decrease transport of high CO_2 into N. America, reduction of equatorward transport of high CO_2 air exceeds reduction of poleward transport (blue shading in N. America, Fig. 4c). As a result, synthetic satellite data is depleted in CO_2, in contrast to Experiment 2, and the inversion creates a "sink" over N. America. Meanwhile, poleward mass fluxes, and hence poleward eddy CO_2 transport, is enhanced in eastern Europe in G5F05. This amplifies the fraction of high CO_2 air hidden from satellites and therefore amplifies the "source" found in Experiment 2.

4 Conclusions

Upward and poleward frontal CO_2 transport feeds off the background vertical CO_2 gradient, which is modulated by sub-grid vertical transport processes such as cumulus convection and turbulent diffusion. Air masses transported by frontal processes are moist and contain systematically different CO_2 signals from equatorward-moving dry air masses. The implication for source/sink estimation is two-fold. First, CO_2 signals contained in moist air masses are hidden from orbital sensors on satellites. This causes small but systematic errors in regional scale flux retrieval in northern mid-latitudes. Second, moist processes are represented differently in GEOS-4 and GEOS-5, leading to differences in the vertical CO_2 gradient and hence the fraction of moist CO_2 air hidden from satellites. Thus, differences in vertical transport amplify sampling biases, which are then aliased in the inversion through increases in continental scale flux retrieval errors throughout northern mid-latitudes. Specifically, the European source is amplified by 0.43 ± 0.35 PgC yr^{-1} while a weak source in eastern N. America is replaced with a strong sink. These results, cast from the perspective of moist frontal transport processes, support previous arguments that the vertical gradient of CO_2 is a major cause of errors in source/sink inversions.

While these results are important for the interpretation of flux errors associated with satellite observations of CO_2, we caution these errors in no way bracket the possible range of

flux errors to be expected in an inversion of real data. We have eliminated important factors such as transport model, assimilation system, and differences in specific humidity fields between GEOS-4 and GEOS-5, but have not addressed errors due to other differences in experimental setup, in particular the calculation of XCO_2. For example, we have not considered aerosol effects, land surface type, or surface pressure. In the absence of condensation, aerosol effects may be important for frontal transport in urban areas in Europe and eastern N. America or in regions of biomass burning. High aerosol burden could have a similar impact on flux inversions as clouds, and should therefore be a focus of future studies.

We also caution that, while signal detection experiments suggest that two weeks of data assimilation may provide a sufficient constraint for flux inversion of satellite data, our results also suggest that it may contribute to flux biases. If CO_2 is mixed rapidly through the domain then we should expect that flux retrieval is not sensitive to the timescale for data assimilation. If, however, the timescale for transport is long compared to the timescale at which CO_2 is sampled, then biases may be introduced. If the time-scale for meridional transport is greater than two weeks, then a longer window may be preferable. Our experiments assume that greater sampling coverage of satellites would permit shorter assimilation windows; we did not consider, however, that temporal sampling errors associated with moist frontal transport would bias the flux inversion. Future studies should more thoroughly examine sensitivity of satellite inversions to data assimilation window.

There is little doubt in the CO_2 inversion community that priority should be given to improving sub-grid vertical transport. Despite efforts to treat transport error, including joint inversion of column/surface CO_2 and meteorological data (Chevallier et al., 2011; Kang et al., 2011) and implicit accounting for transport errors through Monte Carlo and ensemble approaches (Chavallier et al., 2007; Teixeira et al., 2008; Liu et al., 2011), it is not clear to what extent these techniques fix or exacerbate transport errors. It seems that only better characterized model parameterizations, developed based on extensive in situ meteorological measurements, will help address transport models.

Acknowledgements. This research is supported by NASA Carbon Cycle Science and NASA grants NNX08AM56G and MAP/04-0085-0081.

Edited by: M. Heimann

References

Baker, D. F., Bösch, H., Doney, S. C., O'Brien, D., and Schimel, D. S.: Carbon source/sink information provided by column CO_2 measurements from the Orbiting Carbon Observatory, Atmos. Chem. Phys., 10, 4145–4165, doi:10.5194/acp-10-4145-2010, 2010.

Bloom, S. C., Takacs, L. L., Da Silva, A. M., and Ledvina, D.: Data assimilation using incremental analysis updates, Mon. Weather Rev., 124, 1256–1271, 1996.

Bloom, S., da Silva, A., and Dee, D.: Documentation and Validation of the Goddard Earth Observing System (GEOS) Data Assimilation System – Version 4. Technical Report Series on Global Modeling and Data Assimilation, in: Global Modeling Data Assimilation 104606, Tech. Rep. Ser. 26, NASA Goddard Space Flight Cent., Md., 2005.

Bruhwiler, L. M. P., Michalak, A. M., Peters, W., Baker, D. F., and Tans, P.: An improved Kalman Smoother for atmospheric inversions, Atmos. Chem. Phys., 5, 2691–2702, doi:10.5194/acp-5-2691-2005, 2005.

Chevallier, F., Breon, F.-M., and Rayner, P. J.: Contribution of the Orbiting Carbon Observatory to the estimation of CO_2 sources and sinks: Theoretical study in a variational data assimilation framework, J. Geophys. Res., 112, D09307, doi:10.1029/2006JD007375, 2007.

Chevallier, F., Maksyutov, S., Bousquet, P., Breon, F.-M., Saito, R., Yoshida, Y., and Yokota, T.: On the accuracy of the CO_2 surface fluxes to be estimated from the GOSAT observations. Geophys. Res. Lett., 36, L19807, doi:10.1029/2009GL040108, 2009.

Chevallier, F., Feng, L., Boesch, H., Palmer, P., and Rayner, P.: On the impact of transport model errors for the estimation of CO_2 surface fluxes from GOSAT observations, Geophys. Res. Lett., 37, L21803, doi:10.1029/2010GL044652, 2010.

Chevallier, F., Deutscher, N. M., Conway, T. J., Ciais, P., Ciattaglia, L., Dohe, S., Fröhlich, M., Gomez-Pelaez, A. J., Griffith, D., Hase, F., Haszpra, L., Krummel, P., Kyrö, E., Labuschagne, C., Langenfelds, R., Machida, T., Maignan, F., Matsueda, H., Morino, I., Notholt, J., Ramonet, M., Sawa, Y., Schmidt, M., Sherlock, V., Steele, P., Strong, K., Sussmann, R., Wennberg, P., Wofsy, S., Worthy, D., Wunch, D., and Zimnoch, M.: Global CO_2 fluxes inferred from surface air-sample measurements and from TCCON retrievals of the CO_2 total column, Geophys. Res. Lett., 38, L24810, doi:10.1029/2011GL049899, 2011.

Cohn, S. E., Da Silva, A., Guo, J., Sienkiewicz, M., and Lamich, D.: Assessing the effects of data selection with the DAO physical-space statistical analysis system, Mon. Weather Rev., 126, 2913–2926, 1998.

Collins, N., Theurich, G., DeLuca, C., Suarez, M., Trayanov, A., Balaji, V., Li, P., Yang, W., Hill, C., and da Silva, A.: Design and implementation of components in the Earth System Modeling Framework, Int. J. High Perf. Comput. Appl., 19, 341–350, doi:10.1177/1094342005056120, 2005.

Corbin, K. D. and Denning, A. S.: Using continuous data to estimate clear-sky errors in inversions of satellite CO_2 measurements, Geophys. Res. Lett., 33, L12810, doi:10.1029/2006GL025910, 2006.

Corbin, K. D., Denning, A. S., Wang, J.-W., Lu, L., Prihodko, L., and Baker, I. T.: Possible representation errors in inversions of satellite CO_2 retrievals, J. Geophys. Res., 113, D02301, doi:10.1029/2007JD008716, 2008.

Crisp, D., Fisher, B. M., O'Dell, C., Frankenberg, C., Basilio, R., Bösch, H., Brown, L. R., Castano, R., Connor, B., Deutscher, N. M., Eldering, A., Griffith, D., Gunson, M., Kuze, A., Mandrake, L., McDuffie, J., Messerschmidt, J., Miller, C. E., Morino, I., Natraj, V., Notholt, J., O'Brien, D. M., Oyafuso, F., Polonsky, I., Robinson, J., Salawitch, R., Sherlock, V., Smyth, M., Suto, H., Taylor, T. E., Thompson, D. R., Wennberg, P. O., Wunch, D., and Yung, Y. L.: The ACOS CO_2 retrieval algorithm – Part II: Global X_{CO_2} data characterization, Atmos. Meas. Tech., 5, 687–707, doi:10.5194/amt-5-687-2012, 2012.

Denning, A. S., Holzer, M., Gurney, K. R., Heimann, M., Law, R. M., Rayner, P. J., Fung, I. Y., Fan, S., Taguchi, S., Friedlingstein, P., Balkanski, Y., Taylor, J., Maiss, M., and Levin, I.: Three-dimensional transport and concentration of SF6: A model intercomparison study (TransCom 2), Tellus B, 51, 266–297, 1999.

Eguchi, N. and Yokota, T.: Investigation of clear-sky occurrence rate estimated from CALIOP and MODIS observations, Geophys. Res. Lett., 35, L23816, doi:10.1029/2008GL035897, 2008.

Gurney, K., Law, R. M., Denning, A. S., Rayner, P. J., Baker, D., Bousquet, P., Bruhwiler, L., Chen, Y.-H., Ciais, P., Fan, S., Fung, I. Y., Gloor, M., Heimann, M., Higuchi, K., John, J., Maki, T., Maksyutov, S., Masarie, K., Peylin, P., Prather, M., Pak, B. C., Randerson, J., Sarmiento, J., Taguchi, S., Takahashi, T., and Yuen, C.-W.: Towards robust regional estimates of CO_2 sources and sinks using atmospheric transport models, Nature, 415, 626–630, 2002.

Hack, J. J.: Parameterization of moist convection in the National Center for Atmospheric Research community climate model (CCM2), J. Geophys. Res., 99, 5551–5568, 1994.

Holtslag, A. A. M. and Boville, B. A.: Local versus non-local boundary layer diffusion in a global climate model, J. Climate, 6, 1825–1842, 1993.

Houweling, S., Aben, I., Breon, F.-M., Chevallier, F., Deutscher, N., Engelen, R., Gerbig, C., Griffith, D., Hungershoefer, K., Macatangay, R., Marshall, J., Notholt, J., Peters, W., and Serrar, S.: The importance of transport model uncertainties for the estimation of CO_2 sources and sinks using satellite measurements, Atmos. Chem. Phys., 10, 9981–9992, doi:10.5194/acp-10-9981-2010, 2010.

Kang, J. S., Kalnay, E., Liu, J., Fung, I., Miyoshi, T., and Ide, K.: "Variable localization" in an ensemble Kalman filter: Application to the carbon cycle data assimilation, J. Geophys. Res., 116, D09110, doi:10.1029/2010JD014673, 2011.

Kawa, S. R., Erickson III, D. J., Pawson, S., and Zhu, Z.: Global CO_2 transport simulations using meteorological data from the NASA data assimilation system, J. Geophys. Res., 109, D18312, doi:10.1029/2004JD004554, 2004.

Keppel-Aleks, G., Wennberg, P. O., and Schneider, T.: Sources of variations in total column carbon dioxide, Atmos. Chem. Phys., 11, 3581–3593, doi:10.5194/acp-11-3581-2011, 2011.

Kiehl, J. T., Hack, J. J., Bonan, G. B., Boville, B. A., Williamson, D. L., and Rasch, P. J.: The National Center for Atmospheric Research Community Climate Model: CCM3, J. Climate, 11, 1131–1149, 1998.

Kuze, A., Suto, H., Nakajima, M., and Hamazaki, T.: Thermal and near infrared sensor for carbon observation Fourier-transform spectrometer on the Greenhouse Gases Observing Satellite for greenhouse gases monitoring, Appl. Optics, 48, 6716–6733, doi:10.1364/AO.48.006716, 2009.

Lauvaux, T., Pannekoucke, O., Sarrat, C., Chevallier, F., Ciais, P., Noilhan, J., and Rayner, P. J.: Structure of the transport uncertainty in mesoscale inversions of CO_2 sources and sinks using ensemble model simulations, Biogeosciences, 6, 1089–1102, doi:10.5194/bg-6-1089-2009, 2009.

Law, R. M., Chen, Y.-H., Gurney, K. R., and TransCom 3 Modellers: TransCom 3 CO_2 inversion intercomparison: 2. Sensitivity of annual mean results to data choices, Tellus, 55B, 580–595, 2003.

Lin, S.-J.: A "Vertically Lagrangian" finite-volume dynamical core for global models, Mon. Weather Rev., 132, 2293–2307, 2004.

Liu, J., Fung, I., Kalnay, E., and Kang, J.-S.: CO_2 transport uncertainties from the uncertainties in meteorological fields, Geophys. Res. Lett., 38, L12808, doi:10.1029/2011GL047213, 2011.

Lock, A. P., Brown, A. R., Bush, M. R., Martin, G. M., and Smith, R. N. B.: A new boundary layer mixing scheme. Part I: Scheme description and single-column model tests, Mon. Wea. Rev., 138, 3187–3199, 2000.

Lokupitiya, R. S., Zupanski, D., Denning, A. S., Kawa, S. R., Gurney, K. R., and Zupanski, M.: Estimation of global CO_2 fluxes at regional scale using the maximum likelihood ensemble filter, J. Geophys. Res., 113, D20110, doi:10.1029/2007JD009679, 2008.

Louis, J., Tiedtke, M., and Geleyn, J.: A short history of the PBL parameterization at ECMWF, Proc. ECMWF Workshop on Planetary Boundary Layer Parameterization, Reading, United Kingdom, ECMWF, 59–80, 1982.

Moorthi, S. and Suarez, M. J.: Relaxed Arakawa-Schubert: A parameterization of moist convection for general circulation models, Mon. Weather Rev., 120, 978–1002, 1992.

Ott, L. E., Bacmeister, J., Pawson, S., Pickering, K., Stenchikov, G., Suarez, M., Huntrieser, H., Loewenstein, M., Lopez, J., and Xueref-Remy, I.: Analysis of convective transport and parameter sensitivity in a single column version of the Goddard earth observation system, version 5, general circulation model, J. Atmos. Sci., 66, 627–646, 2009.

Parazoo, N. C., Denning, A. S., Kawa, S. R., Corbin, K. D., Lokupitiya, R. S., and Baker, I. T.: Mechanisms for synoptic variations of atmospheric CO_2 in North America, South America and Europe, Atmos. Chem. Phys., 8, 7239–7254, doi:10.5194/acp-8-7239-2008, 2008.

Parazoo, N., Denning, A. S., Berry, J., Wolf, A., Randall, D., Kawa, S. R., Pauluis, O., and Doney, S. C.: Moist synoptic transport of CO_2 along the mid-latitude storm track, Geophys. Res. Lett., 38, L09804, doi:10.1029/2011GL047238, 2011.

Pauluis, O., Czaja, A., and Korty, R.: The global atmospheric circulation on moist isentropes, Science, 321, 1075–1078, 2008.

Pawson, S., Stajner, I., Kawa, S. R., Hayashi, H., Tan, W.-W., Nielsen, J. E., Zhu, Z., Chang, L.-P., and Livesey, N. J.: Stratospheric transport using 6-h-averaged winds from a data assimilation system, Geophys. Res. Lett., 112, D23103, doi:10.1029/2006JD007673, 2007.

Peters, W., Miller, J. B., Whitaker, J., Denning, A. S., Hirsch, A., Krol, M. C., Zupanksi, D., Bruhwiler, L., and Tans, P. P.: An ensemble data assimilation system to estimate CO_2 surface fluxes from atmospheric trace gas observations, J. Geophys. Res., 110, D24304, doi:10.1029/2005JD006157, 2005.

Peylin, P., Bousquet, P., Le Quere, C., Sitch, S., Friedlingstein, P., McKinley, G., Gruber, N., Rayner, P., and Ciais, P.: Multiple constraints on regional CO_2 flux variations over

land and oceans, Global Biogeochem. Cy., 19, GB1011, doi:10.1029/2003GB002214, 2005.

Rienecker, M. M., Suarez, M. J., Todling, R., Bacmeister, J., Takacs, L., Liu, H.-C., Gu, W., Sienkiewicz, M., Koster, R. D., Gelaro, R., Stajner, I., and Nielsen, E.: The GEOS-5 Data Assimilation System – Documentation of Versions 5.0.1, 5.1.0, and 5.2.0. Technical Report Series on Global Modeling and Data Assimilation 104606, 27, 92 pp., 2008.

Rienecker, M. M., Suarez, M. J., Gelaro, R., Todling, R., Bacmeister, J., Liu, E., Bosilovich, M. G., Schubert, S. D., Takacs, L., Kim, G. K., Bloom, S., Chen, J., Collins, D., Conaty, A., da Silva, A., Gu, W., Joiner, J., Koster, R. D., Lucchesi, R., Molod, A., Owens, T., Pawson, S., Pegion, P., Redder, C. R., Reichle, R., Robertson, F. R., Ruddick, A. G., Sienkiewicz, M., and Woollen, J.: MERRA: NASA's Modern-Era Retrospective Analysis for Research and Applications, J. Climate, 24, 3624–3648, doi:10.1175/JCLI-D-11-00015.1, 2011.

Schuh, A. E., Denning, A. S., Corbin, K. D., Baker, I. T., Uliasz, M., Parazoo, N., Andrews, A. E., and Worthy, D. E. J.: A regional high-resolution carbon flux inversion of North America for 2004, Biogeosciences, 7, 1625–1644, doi:10.5194/bg-7-1625-2010, 2010.

Stephens, B. B. Gurney, K. R., Tans, P. P., Sweeney, C., Peters, W., Bruhwiler, L., Ciais, P., Ramonet, M., Bousquet, P., Nakazawa, T., Aoki, S., Machida, T., Inoue, G., Vinnichenko, N., Lloyd, J., Jordan, A., Heimann, M., Shibistova, O., Langenfelds, R. L., Steele, L. P., Francey, R. J., and Denning, A. S.: Weak northern and strong tropical land carbon Uptake from vertical profiles of atmospheric CO_2, Science, 316, 1732–1735, 2007.

Teixeira, J. and Reynolds, C. A.: Stochastic nature of physical parameterization in ensemble prediction: A stochastic convection approach, Mon. Weather Rev., 136, 483–496, doi:10.1175/2007MWR1870.1, 2008.

Wu, W.-S., Purser, R. J., and Parrish, D. F.: Three-Dimensional Variational Analysis with Spatially Inhomogeneous Covariances, Mon. Weather Rev., 130, 2905–2916, 2002.

Yang, Z., Washenfelder, R. A., Keppel-Aleks, G., Krakauer, N. Y., Randerson, J. T., Tans, P. P., Sweeney, C., and Wennberg, P. O.: New constraints on northern hemisphere growing season net flux, Geophys. Res. Lett., 34, L12807, doi:10.1029/2007GL029742, 2007.

Yi, C., Davis, K. J., Bakwin, P. S., Denning, A. S., Zhang, N., Desai, A., Lin, J. C., and Gerbig, C.: Observed covariance between ecosystem carbon exchange and atmospheric boundary layer dynamics at a site in northern Wisconsin, J. Geophys. Res., 109, D08302, doi:10.1029/2003JD004164, 2004.

Zhang, G. J. and McFarlane, N. A.: Sensitivity of climate simulations to the parameterization of cumulus convection in the Canadian climate center general-circulation model, Atmos. Ocean, 33, 407–446, 1995.

Zupanski, D., Denning, A. S., Uliasz, M., Zupanski, M., Schuh, A. E., Rayner, P. J., Peters, W., and Corbin, K. D.: Carbon flux bias estimation employing Maximum Likelihood Ensemble Filter (MLEF), J. Geophys. Res., 112, D17107, doi:10.1029/2006JD008371, 2007.